

Vibrational properties and phase transitions in Lithium doped fullerenes

L. CRISTOFOLINI, M.P. FONTANA

INFN and Department of Physics, University of Parma

Parco Area delle Scienze 7/A, 43100 Parma, ITALY

We review the results of our recent investigations on the structure of the heavily doped fullerene $\text{Li}_{12}\text{C}_{60}$, as determined by high resolution XRD, and on the dynamics of both the C_{60} units and of the Li ions, as it emerges from a variety of experimental techniques: ^{13}C and ^7Li NMR, Raman scattering and Quasielastic Neutron Scattering. The emerging picture is that $\text{Li}_{12}\text{C}_{60}$ at high temperature has the same FCC structure and the same dynamical features as pure C_{60} with the only addition of Li localised diffusion within the octahedral void in the C_{60} structure. As the temperature is lowered, Li diffusion is hindered and a structural transition is induced to a phase of lower than cubic symmetry, which is characterised by the disappearance of overall C_{60} librations and Li diffusion and broadening of the localised molecular excitations of C_{60} , as detected by QENS.

1 Introduction

Lithium doping of fullerene has recently attracted special attention^{1,2,3} also because of subtle structural and charge transfer effects that take place in alkali metal doped fullerenes A_xC_{60} ($\text{A} =$ alkali metal, $x=1,3,4,6,\dots$) when the radius of the alkali metal is much smaller than the typical radii r of the tetrahedral and octahedral voids of the pristine C_{60} pseudo-cubic structure ($r=1.12\text{\AA}$ and $r=2.06\text{\AA}$ respectively). In large radius alkali metal doped fullerenes ($\text{A}=\text{K}, \text{Rb}, \text{Cs}$) the crystal structure can be modelled (with the only exception of A_1C_{60}) as intercalation of the alkali metal ions into the pristine C_{60} cubic structure. Moreover, these compounds show full electronic transfer from the alkali metal ion to the C_{60} unit, thus the stoichiometric parameter x reflects the charge state of the C_{60} unit.

This class of materials has commanded much interest because of its superconducting and magnetic properties⁴: for instance A_1C_{60} compounds are cubic at high temperature, while the low temperature equilibrium phase displays unusual 1-D polymeric chains⁵ confirmed by the presence of a distinct inter- C_{60} vibrational signature of polymeric bond^{6,7}, moreover A_1C_{60} supports a magnetic spin density wave transition^{8,9} below $T=50\text{K}$.

A_3C_{60} compounds display superconductivity ($T_c=33\text{K}$ in $\text{Cs}_2\text{RbC}_{60}$, ref 10) with a positive correlation between the critical temperature T_c and the lattice parameter a (which can be varied by choosing the radius of the dopant alkali metal ion), in agreement with BCS-LDA predictions¹¹. For all these compounds a natural limit in the doping level is reached at $x=6$ due to the complete occupancy of the voids of the pristine cubic structure. Such limit is absent when doping with small radius alkali metals (Li and Na, ionic radii= 0.63, 0.97 \AA respectively) which may yield phases with higher alkali metal content, perhaps due to their tendency to form metallic clusters located in the voids of the pseudo cubic fullerene structure, as is the case of $\text{Na}_{11}\text{C}_{60}$ ^{12,13}. In addition, in the case of Na and Li doping there are indications that the charge transfer from the alkali metals to the C_{60} unit is only partial^{1,3,13}, which might imply co-ordination between the alkali metal and the C_{60} units.

Parrinello and co-workers¹⁴, based on Car-Parrinello first principles molecular dynamics calculations, proposed that $\text{Li}_{12}\text{C}_{60}$ could be a stable, highly symmetric fullerene cluster, a 'superfulleroid', with the 12 Li ions coordinated with the 12 pentagonal faces of C_{60} thus preserving the icosahedral I_h symmetry. Clearly such a system should have an interesting dynamics, in particular due to the coupling of the large C_{60} molecules to the intercalated Li ions: vibrational, librational and diffusional motions of both compo-

nents could mix and influence each other yielding quite complex behaviour, and influence both the structure and phase transitions in this material. In this paper, we report structural and dynamical studies in this complex and interesting system.

In the following section 2 we report on the sample preparation and experimental setup, in section 3 we report on NMR and high resolution x-ray diffraction experiments which show that the stoichiometric compound $\text{Li}_{12}\text{C}_{60}$ represents a single phase, stable Li doped fulleride, and determine its crystal structure as a function of the temperature. In section 4 we employ Raman and Inelastic Neutron Scattering to focus on the high energy, localised dynamics of the C_{60} molecular units, while section 5 is devoted to analysis of the QENS data which suggest a dynamical model in which the Li ions diffuse in the confined environment of the octahedral void of the pristine C_{60} molecule, in agreement with the structural information. In conclusion, the emerging picture is that $\text{Li}_{12}\text{C}_{60}$ at high temperature has the same FCC structure and the same dynamical features as pure C_{60} with the only addition of Li localised diffusion within the octahedral void, while at lower temperature the Li diffusion is reduced, resulting in a pseudo-tetragonal phase which is dynamically characterised by a broadening and disappearance of many dynamical features, i.e. of the Li diffusion and of the C_{60} librations and molecular modes.

2 Sample preparation and experimental techniques.

The samples were prepared according to procedures already discussed in the literature¹⁵. The samples for XRD and Raman measurements were sealed in glass or quartz capillaries; those for neutron scattering were sealed in an air-tight (lead-sealed) Aluminium sample holder whose dimensions were optimised for the sample quantity (450 mg) and the neutron beam size. Isotopically pure ^7Li (>99.9%) was required for the neutron scattering experiments in order to avoid the huge neutron absorption cross section of ^6Li present in the natural fraction.

The solid state NMR experiments were performed using a Bruker CXP200 spectrometer ($H_0=4.7\text{T}$, temperature range from 110K to 373K).

X-ray diffractograms were collected both with a laboratory equipment (Siemens D500, $\text{Cu K}\alpha$) and with the high resolution diffraction beam line BM16 of ESRF operating at fixed wavelength $\lambda=0.652924(2)$ Å. The sample temperature was stabilized and the capillary was spun around its axis to average out the effect of preferred orientations.

Neutron inelastic scattering measurements were performed at the Institut Laue Langevin, Grenoble using the IN6 time-of-flight (tof) spectrometer, operating in neutron-energy-gain with incident neutron wavelength of 5.12 Å. The sample was placed inside the cryoloop. Typical accumulation time was 12h. The tof spectra were collected over the full range of scattering angles. Corrections were made for the aluminium can contribution by running an empty sample can. Vanadium was used as calibrant, allowing determination of the relative efficiencies of the counters. The measured instrumental resolution at the elastic line was on average FWHM=0.10 meV. In order to avoid contamination by elastic contributions (Bragg peaks and lattice phonons), only six groups, comprising 173 out of a total of 235 tof spectra, were used in the subsequent analysis. The average exchanged momenta Q were 0.39, 0.60, 0.89, 1.10, 1.69 and $1.\text{Å}^{-1}$ for the 6 selected regions. The neutron-weighted vibrational DOS $G(e)$ was obtained summing up the inelastic data from all the regions.

For both X ray and neutron scattering measurements the data were collected as a function of temperature across the structural phase transition. Raman spectra were collected in the back-scattering geometry with a high luminosity monochromator coupled to a LN_2 cooled CCD multichannel detector. Excitation light ($\lambda=632.8$ nm, $W<1\text{mW}$) was cylindrically focused onto the inner wall of the quartz capillary enclosing

the sample. Care was taken to reduce the power density of the sample so that no perceptible damage took place.

3. NMR and X-ray Diffraction.

We characterized a series of samples, with different composition parameter x . The diffraction patterns corresponding to high doping level (i.e. $x=12, 14, 18, 24$) invariably show a single (1,1,1) pseudo cubic reflection at $2\theta \approx 4.6^\circ$, although with different distribution of intensities between low and high angle reflections, and in general can be indexed at first approximation as face centred cubic, as pristine C_{60} . On the contrary, at lower doping levels (i.e. $x=4,6,10$), the diffraction patterns correspond to a mixture of different phases with lower than cubic symmetry. The contamination from metallic lithium can be estimated to be less than a few percent from all the diffraction patterns.

This indicates for $x \geq 12$ a single C_{60} -like phase, while for $x < 12$ we have lower symmetry phases and/or a mixture of phases. Therefore we focused on the $x=12$ composition.

Moreover, the ^7Li NMR spectrum consists of a single narrow resonance, with full width at half maximum of 11 ppm, whose shift with respect to the LiCl:aq resonance is +3 ppm. The line shift is characteristic of Li nuclei in non-metallic states. No further signal is detected in the spectral region extending up to 1500 ppm, while bulk metallic Li is expected at $K_s \approx 930$ ppm. This is a clear indication that Li is not segregated in a metallic form. Incidentally, no NMR signal from metallic Li was found up to the highest studied doping level $\text{Li}_{24}\text{C}_{60}$.

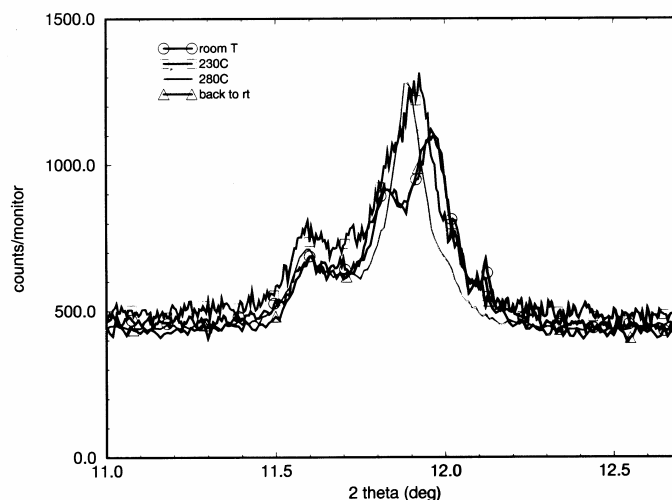


Figure 1: detail of the diffraction pattern of $\text{Li}_{12}\text{C}_{60}$ around the (420) and (331) cubic peaks. The single (420) reflection ($2\theta=11.8^\circ$ at high temperature) is reversibly split when the sample is in the low temperature tetragonal phase.

We collected high-resolution diffraction patterns of $\text{Li}_{12}\text{C}_{60}$ as a function of the temperature in the range 4.2K-550K. While the high temperature diffractograms index as face centred cubic, inspection of the

profiles collected at temperatures below 523K shows a splitting of the pseudo cubic reflections, which can be indexed, in tetragonal symmetry. The splitting increases as the temperature is lowered.

In figure 1 we show the detail of the region around $2\theta=12^\circ$ with the (420) and (331) peaks. All detected low angle reflections imply body centring of the tetragonal cell although a few exceptions are found at high angles. This suggests just a small distortion of the bct cell towards primitive tetragonal, possibly by a displacement of the C_{60} unit from the symmetric $(1/2,1/2,1/2)$ site.

By the Le Bail pattern decomposition technique we obtain, at room temperature, the lattice parameters $a=b=9.894(1)$ Å, and $c=14.209(1)$ Å. Although the Le Bail fit is clearly not a full structural refinement it allows a reliable determination of the cell volume.

As detailed in ref. 16, the diffraction pattern of $Li_{12}C_{60}$ collected on BM16 at $T=553K$ (shown in figure 2) can be indexed in face centred cubic symmetry $Fm\bar{3}m$. Different models were tried for the Rietveld refinement, both with the superfulleroid structure¹⁴ and in the class of the intercalation compounds with an alkali metal cluster in the octahedral void, in analogy with $Na_{11}C_{60}$ in ref. 12. For the ‘superfulleroid structure’, considering the rotational disorder of both C_{60} molecules and of the supposedly attached Li, we modelled it as a simple sphere centred at the origin of the $Fm\bar{3}m$ cell, this model gave invariably a poor fit ($R_{wp} = 19.3\%$, $R_I=8.1\%$, $R_{exp}=2.4\%$).

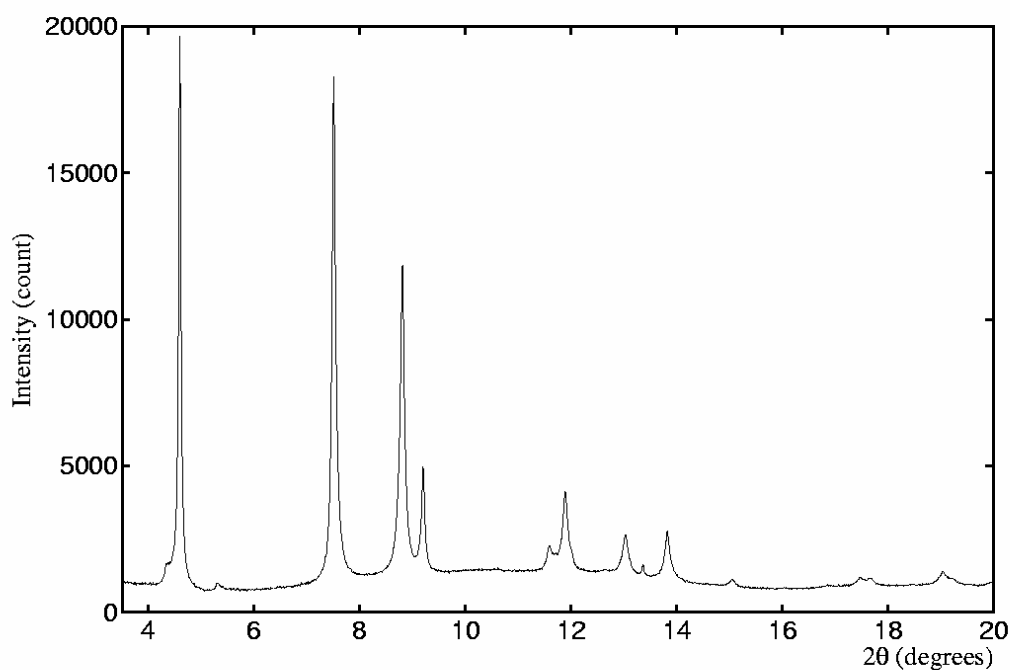


Figure2: Diffraction profile of $Li_{12}C_{60}$ collected on BM16 ($\lambda=0.652924$ Å) at $T=553K$.

The best results were obtained with an intercalation structure. The Profil¹⁷ suite of programs was employed, with a modification that allows modelling the C₆₀ scattering density in terms of symmetry adapted spherical harmonic (SASH) functions¹⁸. The symmetry of the C₆₀ site in the FCC lattice implies that only some of the SASH function coefficients C_{l,v} are non zero, namely those with l=0,6,10,12 and v=1 (plus the term with l=12 and v=2). The 0-th order

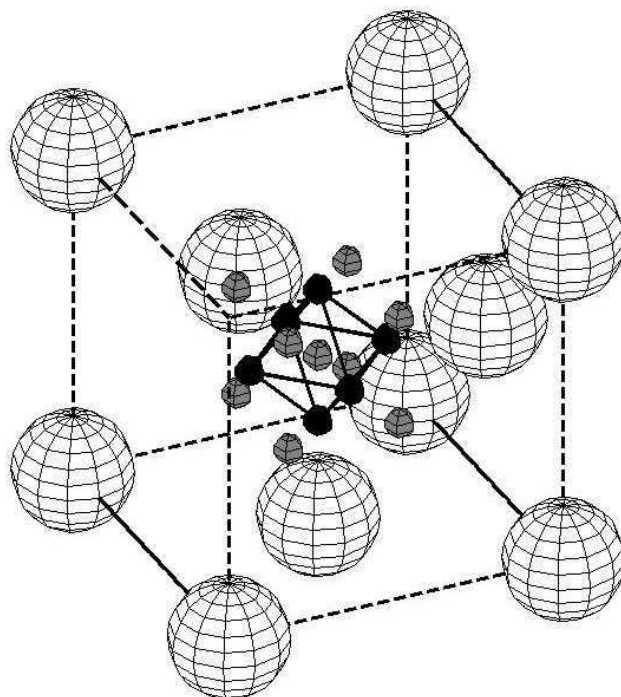


Figure 3: The crystal structure of Li₁₂C₆₀ at T=550K. The C₆₀ units are indicated as large spheres (radius reduced for clarity, not all shown), while the Li ions by the small black (4b and 32f sites) and grey spheres (24e sites) .

corresponds to the spherical contribution, increasing order l corresponds to ‘higher order’ decoration of the sphere. All the Li ions are concentrated in the octahedral voids of the FCC structure:

- i) 4b (1/2, 1/2, 1/2) with almost full occupancy N=3.2(2);
- ii) 32f (x,x,x) x=0.662(1) with full occupancy N= 32(1);
- iii) 24e (1/2, 1/2, y) y=0.690(1), with partial occupancy N=11.3(7).

The isotropic thermal displacement, is B_{iso}=6.6(1.2)Å². The resulting picture is illustrated in figure 3, where the C₆₀ units are indicated as large spheres whose radius is reduced for clarity, while the Li ions by the small black (4b and 32f sites) and grey spheres (24e sites) respectively.

We wish to note here that the value of R=3.559(2)Å is larger than that found in neutral C₆₀ (R=3.5429(6) Å, ref 19), but fully consistent with the radius R=3.556(4)Å (ref 20) of Li₂CsC₆₀. It is indicative of a lengthening of the double bonds as a consequence of the charge transfer onto the C₆₀ molecule. The resulting density of carbon on the C₆₀ sphere, as modelled with the SASH functions, is

maximum in the lattice directions (1,0,0) and (1/2,1/2,1), while it is minimum in the (1,1,1) direction which points towards the tetrahedral void. In other words, there is an excess carbon density in the directions pointing towards all the Li sites and a minimum carbon density in the (1,1,1) direction corresponding to zero occupancy for the tetrahedral site. The situation is somehow analogous in $\text{Li}_2\text{CsC}_{60}$: there²⁰ the negative $C_{10,1}$ value implies an excess of carbon density in the (1,1,1) direction, which corresponds to Li ions residing in the tetrahedral void, here the positive value of the same coefficient correlates with the absence of Li ions in the octahedral void (1,1,1).

4. Raman and Inelastic Neutron Scattering.

It is expected that the phase transition detected by diffraction be accompanied by significant changes also in the molecular excitation spectrum. Therefore, we performed inelastic neutron and light (Raman) scattering on $\text{Li}_{12}\text{C}_{60}$.

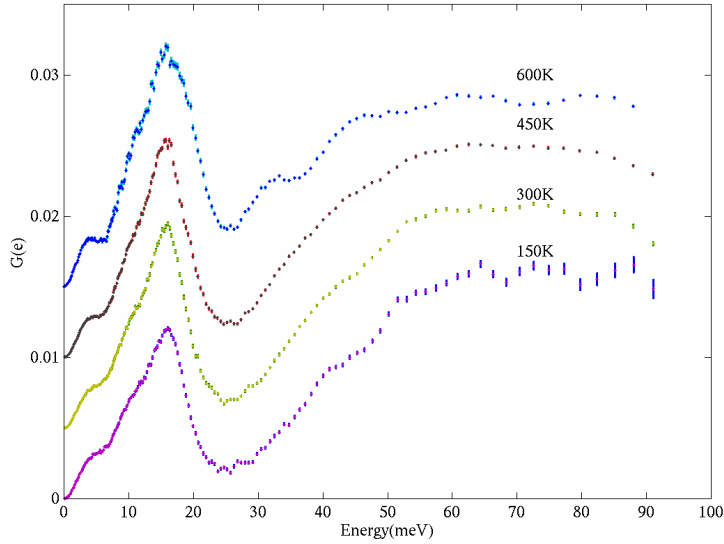


Figure 4: $\text{Li}_{12}\text{C}_{60}$ vibrational density of states $G(e)$ as measured by inelastic neutron scattering as a function of sample temperature.

For the inelastic neutron scattering, within the framework of the incoherent approximation, the spectral distribution function $P(\alpha, \beta)$ is given by

$$P(\alpha, \beta) = 2\beta \sinh(\beta/2) (S(Q, \omega) / \alpha)$$

where $S(Q, \omega)$ is the uncorrected symmetrised scattering law and the dimensionless variables α and β are related to momentum and energy transfer

$$\alpha = \hbar^2 Q^2 / 2Mk_B T$$

$$\beta = \hbar\omega / k_B T$$

where M is an average atomic mass. The experimentally obtained scattering law $S(Q, \omega)$ was converted into the spectral distribution function $P(\alpha, \beta)$ and then corrected for instrumental background, Debye-Waller and multiphonon contributions to yield the neutron-weighted vibrational density of states $G(e)$ using the ILL suite of programmes. As detailed in ref. 21 particular care was used in modelling the theoretical $G(e)$ for the multi-phonon corrections at the higher temperatures. In figure 4 we show the complete vibrational DOS of $\text{Li}_{12}\text{C}_{60}$ measured at $T=600\text{K}$.

The mode originated by the C_{60} 'squashing' $\text{H}_g(1)$ (33 meV), present in the 600K data as a shoulder, disappears completely when going to the lower temperature tetragonal phase. This may indicate that the Li ions clusters act as a "viscous" dampener of the vibrational mode of the C_{60} units, which appear to be freer only at 600K.

Note, on the contrary, the presence of the C_{60} librational peak at 4meV, which survives, as was the case in $\text{Na}_2\text{CsC}_{60}$ (ref 22) and narrows at 600K well above the structural transition into the cubic phase. This is a remarkable result, since for the small Li ions one would expect more diffusional freedom at high temperatures which should lead to at least a dampening of the librational peak.

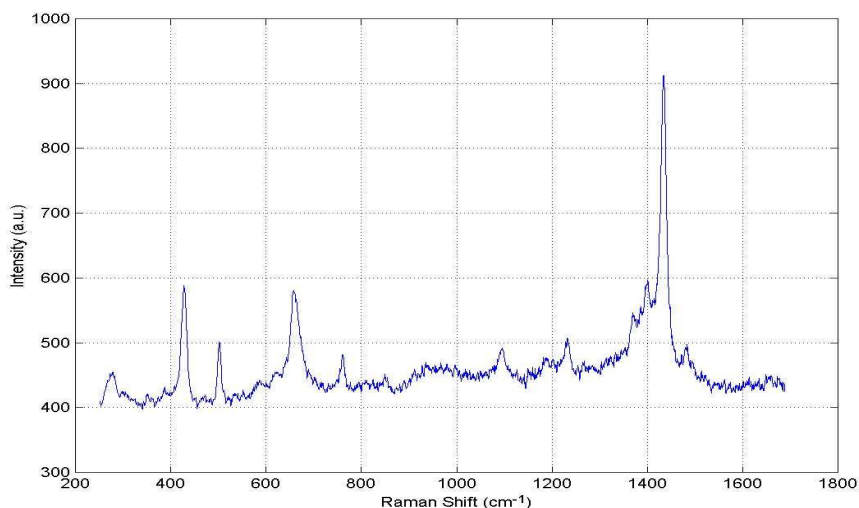


Figure 5: Raman spectrum of $\text{Li}_{12}\text{C}_{60}$ measured at RT with an excitation wavelength $\lambda=632.8$ nm.

The Raman scattering experiment was performed at room temperature; in figure 5 we show the spectrum of $\text{Li}_{12}\text{C}_{60}$ obtained with an integration time of 300sec. The peak positions are reported in Table 1, where we report also the energies of the corresponding molecular excitations in pristine C_{60} and in the fully alkali metal doped fullerenes Rb_6C_{60} at room temperature.

The overall spectrum presents many striking similarities with that of the insulating 6-fold ionised A_6C_{60} ($A= \text{K}, \text{Rb}, \text{Cs}$)²³. Perhaps the most significant information is given by the 'pentagonal pinch' $\text{A}_{g(2)}$ mode, which is a standard indicator of the charge state of the C_{60} unit²⁴, as it softens from 1469cm^{-1} in pristine C_{60} , down to 1445cm^{-1} in K_3C_{60} and to 1432.5cm^{-1} in the fully doped²³ A_6C_{60} .

In $\text{Li}_{12}\text{C}_{60}$ the same $A_{g(2)}$ mode is found at 1432 cm^{-1} again suggesting that the C_{60} unit is 6-fold ionised, in agreement with the idea that the Li ion donates on average only $\frac{1}{2}$ electron¹.

$\text{Li}_{12}\text{C}_{60}$	276	425	503	658	760	1094	1184	1231	1365	1397	1432	1482
Rb_6C_{60}	271	429	500	658	761	1092	1120	1238	1385	1419	1432.5	1484
C_{60}	270	430	493	708	772	1099	Abs.	1248	Abs.	1426	1468.5	1573

Table 1: Raman peak positions (in cm^{-1}) of the molecular excitations in $\text{Li}_{12}\text{C}_{60}$ and in the fully alkali metal doped fullerenes Rb_6C_{60} and in pristine C_{60} at room temperature, from ref. 23.

All the other spectral features found in $\text{Li}_{12}\text{C}_{60}$ are encountered in Rb_6C_{60} also, except perhaps in the spectral region of the high frequency tangential modes, between 1350 and 1432 cm^{-1} , where we find several split lines of intensity much lower than the $A_{g(2)}$ mode, which are not easily resolved by our intermediate-resolution spectrometer. They are indeed indicators of symmetry splitting arising from the locations of the Li ions around the C_{60} unit.

5. Quasielastic Neutron Scattering.

In order to get a better understanding of the cubic to tetragonal phase transition from the point of view of the diffusive dynamics of the Li ions and of the re-orientational diffusion of the C_{60} units we analysed the Quasielastic (QE) neutron scattering signal.

As better detailed in ref. 25 the total scattered intensity was fitted with a two-component model, the elastic intensity being represented by a delta function and the QE intensity by a Lorentzian function both convoluted with the resolution function. The elastic peak intensity is ascribed to the combination of the coherent scattering from the carbon of the C_{60} units and of the Li ions. On the contrary, the QE intensity can not be ascribed to C_{60} , as at low temperature the fullerenes units are blocked, as it emerges from the analysis of the structure and is confirmed by the observation of the full chemical shift anisotropy in the ^{13}C NMR spectrum¹⁶. At high temperature also the QE signal cannot originate from the C_{60} 's, as they perform well-defined librations, as pointed out in the previous section. Therefore, the QE signal must arise from Li ions diffusional motion.

The intensity of the QE signal decreases on cooling from 600K to 450K but does not completely disappear even at the lowest temperatures studied, signifying a residual diffusional motion of the Li ions even in the low temperature regime.

Moreover, the aforementioned observation of C_{60} librations in the FCC phase indicates that the Li ions are not totally free to diffuse between different voids of the crystalline structure, which would result in a smearing of the re-orientational potential felt by the C_{60} units.

The width of the QE signal is about 0.29 meV, independent of the exchanged momentum Q . From this we deduce that the diffusional motion must be localized at least when studied on the space scale of the IN6 experiment, that is between 3 and 16 \AA from the posed limits in Q -space.

At the same time the elastic intensity follows the normal Debye-Waller behaviour from which we obtain the mean square displacement $\langle u^2 \rangle$ associated to the Li ions: $\langle u^2 \rangle = 0.084(14)\text{ \AA}^2$, in good agreement

with the value $\langle u^2 \rangle = 0.083(15) \text{ \AA}^2$ obtained from the high resolution x-ray diffraction. Therefore we used the same Debye-Waller factor to correct the QE intensity, which could then be fitted to a theoretical diffusion model for the motion of the Li ions.

In order to develop a detailed model for the Li diffusion we first identify the sites that participate to the ionic diffusion. These are the 24e sites described in section 2 of the present work, due to their loose occupancy ($N \approx 1/2$) which is required for effective contribution to jump diffusion. We recall that the 24e sites form an octahedron centred at the crystal positions $(1/2, 1/2, 1/2)$. Within such model of octahedral jumps in a confined geometry²⁶ the quasielastic intensity consists of two Lorentzian terms

$$A_1(Q) = 1/3 [1 - 2j_0(\sqrt{2} Q r) + j_0(2Qr)]$$

$$A_2(Q) = 1/2 [1 - j_0(\sqrt{2} Q r)]$$

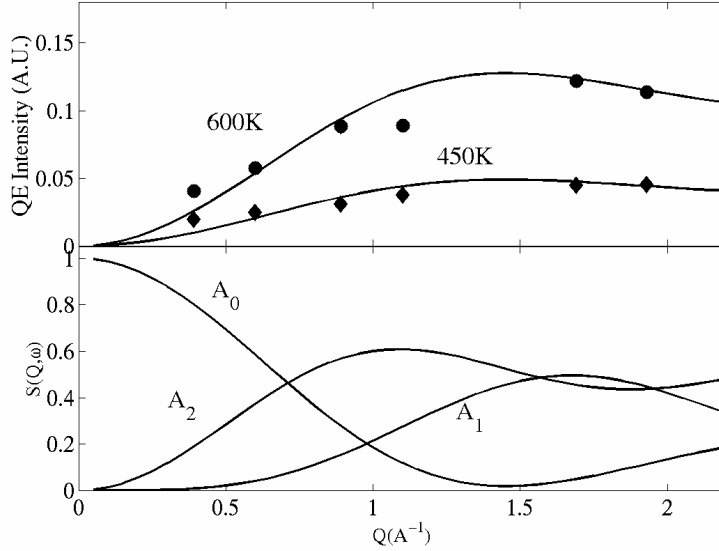


Figure 6: Top panel: elastic (A_0) and inelastic (A_1, A_2) contributions to the scattering law $S(Q, \omega)$ calculated for a particle performing jumps on the vertices of an octahedron (see text). Bottom panel: Q dependence of the QE intensity, after Debye-Waller correction, at $T=600\text{K}$ and $T=450\text{K}$. The lines represent the theoretical fit to octahedral jumps as described in the text

where j_0 is the spherical Bessel function of order 0, and r is the radius of the sphere containing the sites. The two QE widths are $\omega_1 = 1.5/\tau$ and $\omega_2 = 1/\tau$ respectively, τ being the residence time of the particle on each site. Even if the two QE terms display different Q dependence, in the Q range of interest to our IN6 experiment, the complete QE scattering function can be approximated- with an accuracy of 5%- to a single Lorentzian of average width $\langle \omega \rangle = 1.19/\tau$.

In Figure 6 we show the behaviour of the QE intensity, after Debye-Waller correction, for two different temperatures, respectively below and above the phase transition, and the corresponding theoretical fit, with $r= 2.06 \text{ \AA}$, which coincides nicely with the radius of the octahedral void. From the width of the QE intensity the value of the residence time $\tau= 2.7 \pm 0.5\text{ps}$ can be estimated at $T=600\text{K}$. Here we wish to note that the measured residence time is, within the experimental accuracy, independent of temperature across the phase transition. This indicates that the temperature acts only on the number of ions which diffuse according to the rotational diffusion model we propose; once the Li ions are freed to move, they move with the given mobility determined by the local environment, which changes very little across the phase transition.

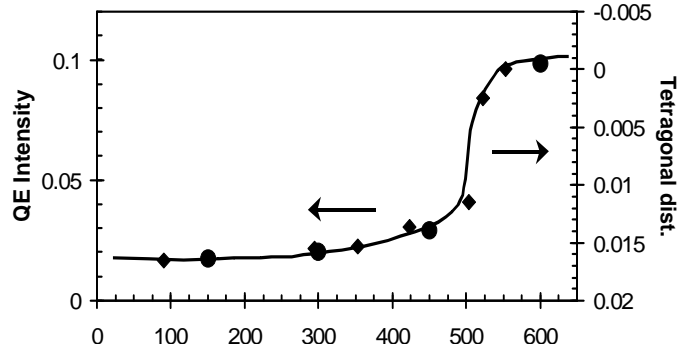


Figure 7: Temperature dependence of the neutron QE intensity at $\langle Q \rangle = 1.10 \text{ \AA}^{-1}$ (and hence of the fraction of Li ions diffusing at a given temperature, circles, left scale) together with the amplitude of the tetragonal distortion in $\text{Li}_{12}\text{C}_{60}$ (diamonds, right scale).

From the ratio of the quasielastic intensities to the corresponding elastic intensity at 600K and 300K we find that the number of diffusing Li ions at 600K is almost 5 times bigger than at 300K. In Fig. 7 we plot the T dependence of the increase of the intensity of the QE signal at $\langle Q \rangle = 1.10 \text{ \AA}^{-1}$ (normalised to the corresponding elastic intensity) with the decrease of the tetragonal distortion of the cubic lattice $(\sqrt{2}a - c) / c$. The two quantities show the same dependence on T. Since the QE intensity is a direct measure of the fraction of Li ions which are free to diffuse, this supports the idea that in the more compact tetragonal phase the Li ions are blocked, while as T is raised the crystal cell expands and more and more Li ions are free to diffuse and therefore contribute to the QE signal.

5 Conclusion

In conclusion, we have reviewed the results of our recent investigations on the structure of a class of heavily doped fullerenes, focusing mainly on the composition $\text{Li}_{12}\text{C}_{60}$. The emerging picture is that $\text{Li}_{12}\text{C}_{60}$ at high temperature has the same FCC structure and the same dynamical features as pure C_{60} with the only addition of Li localised diffusion within the octahedral void in the C_{60} structure. As the temperature is lowered, the Li diffusion is reduced, resulting in a pseudo-tetragonal phase which is dynamically characterised by a broadening and disappearance of many dynamical features, i.e. of the Li diffusion and of the C_{60} librations and molecular modes.

References

1. M. Kosaka, K. Tanigaki, K. Prassides, S. Margadonna, A. Lappas, C.M. Brown, A.N. Fitch, *Phys Rev B* 59, R6628 (1999)
2. T. Yildirim, O. Zhou, and J. Fischer in *Physics and Chemistry of Materials With Low-Dimensional Structures*, Volume on Fullerene based materials; edited by W. Andreoni, (Kluwer Academic Publishers, Dordrecht, 1999).
3. Buhl M., *Z. Anorg. Allg. Chem.*, 2000
4. *The Fullerenes*, edited by H.W. Kroto, J.E. Fischer and E. Cox, (Oxford, Pergamon Press, 1993).
5. P.W. Stephens, G. Bortel, G. Faigel, M. Tegze, A. Janossy, S. Pekker, G. Oszlany, L. Forrò, *Nature*, 370, 636 (1994)
6. L. Cristofolini, C.M. Brown, A.J. Dianoux, M. Kosaka, K. Prassides, K. Tanigaki, K. Vavekis, *J. Chem. Soc., Chemical Communications* 21, 2465 (1996).
7. H. Schober, A. Tolle, B. Renker, R. Heid, F. Gompf, *Phys. Rev. B* 56, 5937 (1997)
8. O. Chauvet, G. Oszlany, L. Forrò, P.W. Stephens, M. Tegze, G. Faigel, A. Janossy, *Phys. Rev. Lett.* 72, 2721 (1994)
9. L. Cristofolini, A. Lappas, K. Vavekis, K. Prassides, R. DeRenzi, M. Ricco, A. Schenck, A. Amato, F.N. Gygax, M. Kosaka, K. Tanigaki, *J. Phys. Cond. Matt.* 7, L567, (1995)
10. K. Tanigaki, T.W. Ebbesen, S. Saito, J. Mizuki, J.S. Tsai, Y. Kubo, S. Kuroshima, *Nature* 352, 222, (1991)
11. K. Prassides, in *Recent Advances in the Chemistry and Physics of Fullerenes and Related Materials* vol 94-24, p 477, edited by K.M. Kadish and R.S. Ruoff, (The Electrochemical Society Inc., Pennington, N.J., 1994)
12. T. Yildirim, O. Zhou, J.E. Fischer, N. Bykovetz, R.A. Strongin, M.A. Cichy, A.B. Smith, C.L. Lin, R. Jelinek, *Nature* 360, 568, (1992)
13. W. Andreoni, P. Giannozzi, J.F. Armbruster, M. Knupfer, J. Fink, *Europhys. Lett.* 34, 699 (1996)
14. J. Kohanoff, W. Andreoni and M. Parrinello, *Chem Phys Lett* 198, 472 (1992)
15. L. Cristofolini, M. Riccò, R. DeRenzi, in *Recent Advances in the Chemistry and Physics of Fullerenes and Related Materials*, vol. 6, p. 687, edited by K.M. Kadish and R.S. Ruoff, (The Electrochemical Society Inc., Pennington, N.J., 1998)
16. L. Cristofolini, M. Riccò, R. De Renzi, *Phys. Rev. B* 59, 8343, (1999)
17. *Profil*, 5.17; J. K. Cockcroft, Birbeck College, London.
18. W. Press A. Huller, *Acta Crystallographica A*, 29, 252 (1973); J. P. Amoreaux, M. Bee, *Acta Crystallographica B*, 36, 2636 (1980); J.K. Cockcroft A. Fitch, *Z. Kristallogr* 184, 123 (1988); K. Prassides, personal communication

19. P.C. Chow, X. Jiang, G. Reiter, P. Wochner, S.C. Moss, J.D. Axe, J.C. Hanson, R.K. McMullan, R.L. Meng, C.W. Chu, *Phys Rev Lett* 69, 2943 (1992)
20. I. Hirosawa, K. Prassides, J. Mizuki, K. Tanigaki, M. Gevaert, A. Lappas, J. K. Cockcroft, *Science* 264, 1294 (1994)
21. L. Cristofolini, G. Cicognani, A.J. Dianoux, P. Facci, M.P. Fontana, M. Riccò, *Philos. Mag.* B79, 2065 (1999)
22. L. Cristofolini, K. Vavekis, K. Prassides, A.J. Dianoux, M. Kosaka, I. Hirosawa, K. Tanigaki, *Physica B* 226, 41 (1996).
23. K.A. Wang, Y. Wang, P. Zhou, J.M. Holden, S. Ren, G.T. Hager, H.F. Ni, P. C. Eklund, G. Dresselhaus, M.S. Dresselhaus *Phys. Rev B*, 45, 1955 (1992).
24. R.C. Haddon, AF Hebard, M.J. Rosseinsky, D.W. Murphy, SJ Duclos, KB Lyons, B Miller, JM Rosamilia, RM Fleming, A.R. Kortan, SH. Glarum, A.V. Makhija, A.J. Muller, R.H. Eick, SM Zahurak, R Tycko, G. Dabbagh, F.A. Thiel. *Nature*, 350, 320 (1991)
25. L. Cristofolini, P. Facci, M.P. Fontana, G. Cicognani, A.J. Dianoux, *Phys Rev B* 61, 3404, (2000)
26. L. Cristofolini, P. Damay, A.J. Dianoux, *Physica B*, in press